09

Effect of the introduction of single-walled carbon nanotubes and reduced graphene oxide on the structure formation and specific resistance of yhydrogels during photopolymerization

© M.S. Savelyev[1,2]

[1]Institute of Biomedical Systems, National Research University of Electronic Technology, „MIET“, 124498 Moscow, Zelenograd, Russia
[2]Institute for Bionic Technologies and Engineering, Sechenov First Moscow State Medical University, Sechenov University, 119991 Moscow, Russia
e-mail: savelyev@bms.zone

Received November 25, 2025
Revised November 25, 2025
Accepted November 25, 2025

The effect of ultrasonic treatment of aqueous dispersions of single-walled carbon nanotubes (SWCNTs) and reduced graphene oxide (RGO) on the structure formation and specific resistivity of photopolymerized biopolymer hydrogels (matrix: collagen/BSA/chitosan/eosin Y) has been studied. For this purpose, dynamic light scattering was used in combination with specific resistivity measurements. The optimal ratio of 1 to 1 for SWCNTs with a hydrodynamic radius of 0.49 μm (80 min treatment) and RGO with 0.21 μm (80 min treatment) provided a specific resistivity of 14 Ω·cm, while hydrogels retain the ability to swell up to 200 %. The analysis of the dependence of temperature and normalized optical transmission on the duration of laser photopolymerization made it possible to determine the optimal temperature of the liquid biopolymer precursor 28 °C, which ensures maximum reproducibility of the specific resistivity of hydrogels produced by photolithography

Keywords: Hydrogel, negative photoresist, temperature, dynamic light scattering, nonlinear absorption cross section, carbon nanotubes, reduced graphene oxide, biocompatibility, neurointerface.

DOI: 10.61011/TP.2026.05.63526.314-25

Introduction

Electrical stimulation accelerates and triggers ionic processes in cells by activating intracellular pathways and ion channels [1,2], which is necessary for therapeutic tissue stimulation [3,4], recovery of nerve conduction [5,6] and chronic pain relief in case of spinal cord injuries [7,8]. To realize these effects, electrodes made of conductive and biocompatible materials are being developed that can deliver necessary energy for a long time to block pain and provide other therapeutic tasks [9–11].

Metal electrodes have limited duration of stable operation due to encapsulation and related problems — signal drift and corrosion [12], skin allergy and inflammation [13], as well as mechanical mismatch of soft nervous tissue [14]. For long-term use, a material with breathability, good adhesion during tissue movement and mechanical flexibility is required [2,3,5,10,11]. In this paper, it is proposed to use conductive hydrogels as an interface between electrodes and a nerve: this increases the stability of neurostimulators for controlling phantom pain and sensitizing bionic devices, and their effectiveness in simulating or enhancing the functions of sensory neurons [15,16].

Hydrogels with sufficient resistivity reduce corrosion of metal electrodes due to the ability to operate at lower currents [12,17–19]. Collagen, bovine serum albumin (BSA), and chitosan are considered as biocompatible matrices, but they do not provide the necessary conductivity by themselves [20,21]. Single-wall nano tubes (SWCNT) are suggested to lower the resistivity; however, the use of SWCNT is a disputable issue because of their known toxicity, therefore, pre-treatment methods are required to achieve their potential while keeping their minimal content [22]. The biocompatible shells (e.g., BSA or chitosan) may reduce the toxicity of SWCNT and provide their good compatibility with tissues [23–25]. In addition, other allotropic forms of carbon sometimes exhibit lower toxicity compared to SWCNT, which makes it possible to increase their proportion in compositions without significantly impairing biocompatibility [24,26]. Earlier in our paper [27], an increase in the current emission was described for the case of graphene and SWCNT combined under the action of laser irradiation to form a recombinant graphene/SWCNT structure. In the present study, to get a homogeneous dispersion, the splitting of SCNT beams by dynamic light scattering (DLS) was controlled and the reduced graphene oxide (RGO) was included in the dispersion.

The resistivity was evaluated for hydrogels formed on the basis of a collagen/BSA/chitosan/eosin Y/SWCNT/RGO dispersion, considered by analogy with a negative photoresist. For successful photopolymerization, the optical characteristics of the system and temperature control are critical [28], to avoid irreversible denaturation of sensitive protein components [29]. Eosin Y was used as a photo-

sensitive component due to its ability to absorb the applied laser radiation [23].

1. Materials and optical research

1.1. Preparation of carbon components

Nano tubes TUBALLTM (OCSiAl, Moscow, Russia) with a 99 wt% product content were selected as SWCNT. Other carbon allotropic materials and metal impurities are less than 1 wt%, with a diameter (1.6 ± 0.4) nm, length over $5\,\mu$m and specific surface area $40\,m^2/g$ [21,30,31]. RGO (OOO „Graphenox“, Chernogolovka, Russia) with a specific surface area of $50\,m^2/g$ was used [32,33]. A stable dispersion was achieved using an ultrasound immersion homogenizer Sonicator Q700 (Qsonica, Newtown, Connecticut, USA) by treatment from 20 to 100 min at frequency of 20 kHz and power of 210 W. Thermostatic cooling was used to prevent boiling. Such ultrasound treatment with an immersion homogenizer impacted the distribution of nanotubes. At the same time, filter paper was used to remove large tangles that can form under the action of van der Waals forces [34,35].

1.2. Preparation of dispersions for fabrication of hydrogel

The dispersion, which can be used like a negative photoresist, was prepared in three stages. Such components as chitosan (OOO „Bioprogress“, Losino-Ostrovsky, Russia), collagen (OOO „MakMedi“, Moscow, Russia) and BSA (BioClot, Aidenbach, Germany) were used. As a result, a uniform distribution of components was achieved throughout the volume. Sodium deoxycholate and acetic acid (Sigma-Aldrich, St. Luis, Missouri, USA) were used as surfactants.

At the first stage, using the magnetic stirrer Elmi MS-01 (ELMI, Riga, Latvia) the aqueous solutions of eosin Y (Agat-Med, Moscow, Russia), BSA and collagen were prepared. In parallel, the dispersions were prepared by ultrasonic treatment, containing carbon components and chitosan in a 10 % vinegar solution, which cannot be sufficiently stirred using a magnetic stirrer.

The second stage involves mixing with the magnetic stirrer the solutions of BSA, collagen and chitosan obtained in the first stage with each other. In parallel, SWCNT, RGO and eosin Y were mixed using a laboratory paddle mixer, allowing to avoid their sticking together as a result of magnetization. In case of carbon nanoparticles, sodium deoxycholate as a surfactant was used in the amount of 1 %.

The third stage involved mixing the samples obtained in the second stage with each other with the paddle mixer. As a result, five dispersion samples were obtained (negative photoresist) containing 2.5 wt% collagen, 5 wt% BSA, 2 wt% chitosan, 0.5 wt% eosin Y, 0.02 wt% RGO, while 0.02 wt% SWCNT had different treatment periods (in parentheses the hydrodynamic radius R of particles with the greatest contribution is indicated): 1 — SWCNT ($R = 0.80\,\mu$m), 2 — SWCNT ($R = 0.60\,\mu$m), 3 — SWCNT ($R = 0.52\,\mu$m), 4 — SWCNT ($R = 0.49\,\mu$m), 5 — SWCNT ($R = 0.55\,\mu$m).

1.3. Optical research and temperature control

HTTP MARK MOPA laser system (DB „Bulat, Zelenograd, Russia) was used as radiation sources in the generation mode (wavelength 1070 nm) with a pulse duration of 120 ns with a pulse repetition period of $67\,\mu$s (Fig. 1). The radiation was incident on the lens to obtain sufficient intensity and non-linear effects. The sample was placed in a holder mounted on a motorized table N31.100E, controlled by PLC E71.D4E-H (CoreMorrow Ltd., Harbin, China) to move along the beam direction towards the second lens. A beam splitter was installed behind these optical components, splitting the beam into two trajectories. In one case, an aperture in front of the power sensor was installed in the radiation path, and in the other, the beam hit the power sensor directly G5F-GT-10 (ShenZhen CaiHuang Thermoelectricity Technology Co. Ltd., Shenzhen, China). This made it possible to conduct Z-scanning and determine optical transmission. In case of plotting the curves of temperatures and normalized transmissions versus time the cuvette with the sample was placed in the focus of the lens. During the research, GM320 pyrometer (Benetech, Inc., Montgomery, IL, USA) and IR USB Camera Module thermal imager (Wuhan Guide Sensmart, ltd., Wuhan, China) were used, which simplified the definition of the area for heating control according to the method we used earlier [28].

Before determining the nonlinear absorption section σ [23,36], the nonlinear absorption coefficient β and the threshold exposure of laser radiation F_x were estimated as per the radiative transfer equation (RTE) [37]:

$$T_{norm} = \exp\left(-\frac{\beta}{\tau}\left(\frac{2U}{w(z)\pi} - F_x\right)d\right), \tag{1}$$

where d — thickness of the cuvette filled with the dispersion; τ — pulse duration in time; U — total energy of a single pulse; $w(z)$ — radius of the beam depending on the displacement of sample z relative to the lens focus, which is determined by the formula [38]:

$$w(z) = w_0\sqrt{1 + \frac{\lambda z^2}{\pi w_0^2}}, \tag{2}$$

where w_0 — radius of constricted beam ($40\,\mu$m); λ — wavelength. Full pulse energy was determined based on the measured laser power P (190 mW):

$$U = PT_p, \tag{3}$$

where T_p — pulse repetition period ($67\,\mu$s).

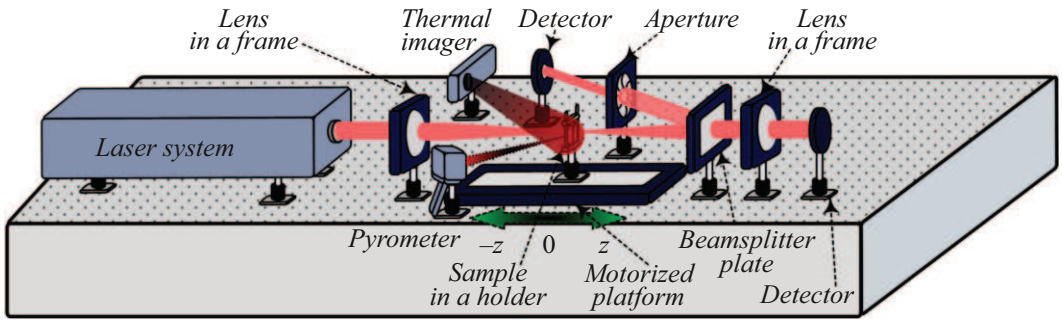

Figure 1. Experimental setup.

As a result, the section of non-linear adsorptionσ is defined using the obtained non-linear adsorption coefficient β by formula [23,36]:

$$\sigma = \frac{\beta \hbar\omega}{N_A C \cdot 10^{-3}}, \tag{4}$$

where $\hbar\omega$ — energy of absorbed photon (0.19 aJ); N_A — Avogadro number; C — concentration (7.2 mmol/L).

To assess the possible effect of scattering, the nonlinear refractive index nn [23,38] was estimated. As a result of measurements using Z-scanning with open and closed apertures, the normalized transmission value was determined:

$$T_{norm} = \frac{16\pi n_n P_0 T_p L_{eff} z \pi \omega_0^2}{\tau \omega_0^2 \pi \sqrt{\pi}(z^2\lambda^2 + 9\pi^2\omega_0^4)(z^2\lambda^2 + \pi^2\omega_0^4)}, \tag{5}$$

where the effective thickness of L_{eff} layer is determined by the linear absorption coefficient — ($40\,\text{cm}^{-1}$) and the cuvette thickness d (1 mm) in accordance with the expression

$$L_{\text{eff}} = \frac{1 - \exp(-\alpha d)}{\alpha}. \tag{6}$$

1.4. Study of resistivity and formation of hydrogel

To assess the resistivity the samples of hydrogels in the form of a square 5×5 mm were prepared. The resistivity values were determined by the van der Pau method. ST2258C setup with a four-probe head unit ST2571A-F01 (Suzhou Jingle Electronics Co., Ltd., Suzhou, China) was used. Photopolymerization was made by laser pulses with a duration of 100 ns with a pulse repetition period of 33 μs using a fiber laser equipped with a scanning system (Fig. 2). The radius of the laser spot in the lens focus was 19 μm. The laser trajectory was set on a PC.

1.5. Swelling estimate

The swelling ability was determined after soaking in isotonic saline solution 5 mL (0.9 % NaCl) at a temperature of 37 °C. The estimate was made based on the results of measurements of initial m_0 value of the sample's dry mass and m_{wt} wet mass. As a result, the degree of swelling S was estimated using the formula [39]:

$$S = \frac{m_{wt}}{m_0} \cdot 100\,\%. \tag{7}$$

2. Results and discussion

2.1. Studies by method of Raman scattering (RS)

Six samples of dispersed media were prepared, which differed in the duration of ultrasonic treatment. Their data are given in Table 1. Characteristic hydrodynamic radius of dispersions with SWCNT and RGO was assessed by RS scattering method.

After 20 min of mixing the hydrodynamic radius for the majority of SWCNT in a dispersion corresponds to $R = 0.8\,\mu$m. As processing progressed over 1 and 60 min, this value decreased to $R = 0.6$ and $0.52\,\mu$m, respectively. This indicates the splitting of the initial beams, which could affect the decrease in the hydrodynamic radius. At the same time, during exposure to powerful ultrasound, the SWCNT may shorten with the formation of many short segments [40], but no increase in the contribution to scattering from them was detected when determining the hydrodynamic radius. The absence of shortening with an increase in the number of defects may occur depending on the choice of ultrasound treatment mode [41]. This effect could be facilitated by a moderate power value of 210 W during processing. By about 80 min, a state close to equilibrium occurs with the value of hydrodynamic radius $R = 0.49\,\mu$m; further processing during 100 min leads to a violation of the decreasing trend and, on the contrary, a slight increase in $R = 0.55\,\mu$m is recorded. During exposure to ultrasound in the specified time range up to 100 min, there is no complete splitting of SWCNT beams and their strong shortening. In case of RGO, the value of hydrodynamic radius of $R = 0.21\,\mu$m was obtained, which indicates their sufficient dispersion and the almost complete absence of clumped flakes (agglomerates).

Further, carbon nanoparticles were used to prepare dispersions, which were intended for use like a negative photoresist.

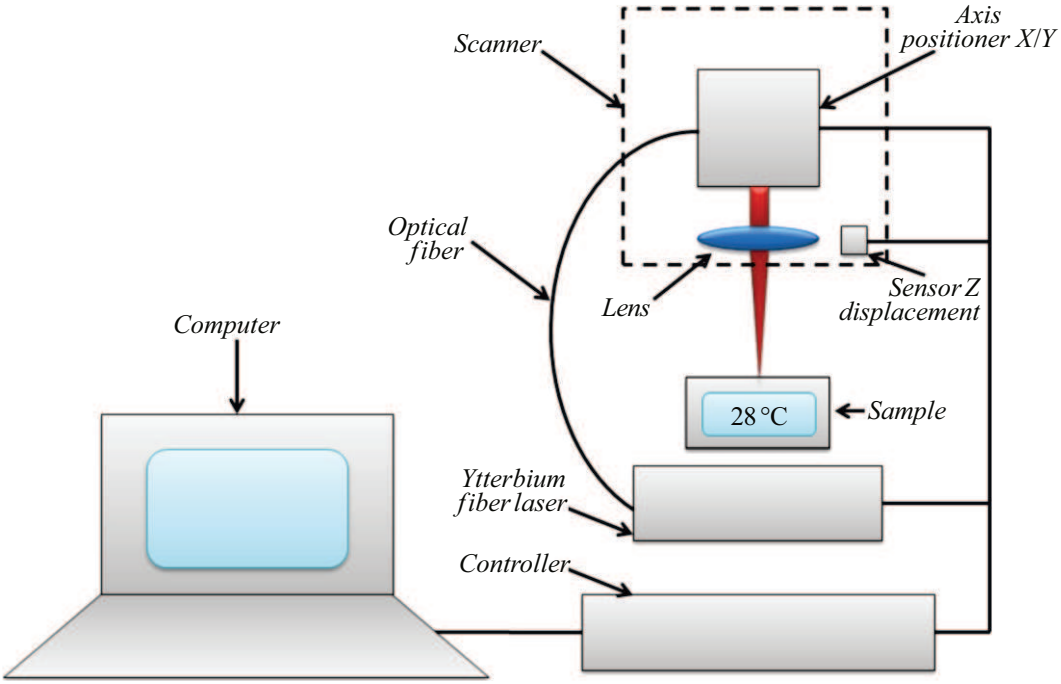

Figure 2. Setup for the photopolymerization of collagen/BSA/chitosan/eosin hydrogel Y/SWCNT/RGO.

Table 1. Data obtained by RS scattering method for SWCNT and RGO

Ultrasonic Time homogenization, min	Carbon Nanoparticles	Hydrodynamic Radius R, μm	Standard deviation, μm	Contribution, %
20	single SWCNT	0.20	0.04	22
	SWCNT beams	0.80	0.24	78
40	single SWCNT	0.07	0.01	7
	SWCNT beams	0.60	0.09	93
60	single SWCNT	0.06	0.01	4
	SWCNT beams	0.52	0.10	96
80	single SWCNT	0.04	0.01	6
	SWCNT beams	0.49	0.10	94
100	single SWCNT	0.07	0.01	7
	SWCNT beams	0.55	0.07	95
80	Single RGO	0.05	0.01	9
	Agglomerates of RGO	0.21	0.05	90

2.2. Temperature and optical density control during photopolymerization

In fabrication of complex shape samples, temperature has a significant effect. To select the temperature during photopolymerization and reduce the number of unpolymerized areas, the effect of laser radiation on the dispersion material (negative photoresist) was studied the material itself was a compound of collagen/BSA/chitosan/eosin Y/SWCNT/RGO, and SWCNT in it had different treatment times (the value of hydrodynamic radius R of particles with the greatest DLS contribution is indicated in parentheses): 1 — SWCNT ($R = 0.8\,\mu$m), 2 — SWCNT ($R = 0.6\,\mu$m), 3 — SWCNT ($R = 0.52\,\mu$m), 4 — SWCNT ($R = 0.49\,\mu$m), 5 — SWCNT ($R = 0.55\,\mu$m). The study results are shown in Fig. 3.

When using pulsed laser radiation with a power of about 190 mW with a pulse repetition period of 67 μs photopolymerization took place for a sufficient time for observation within 100 s. The energy parameters of laser are selected to provide easy measurements. Photopolymer-

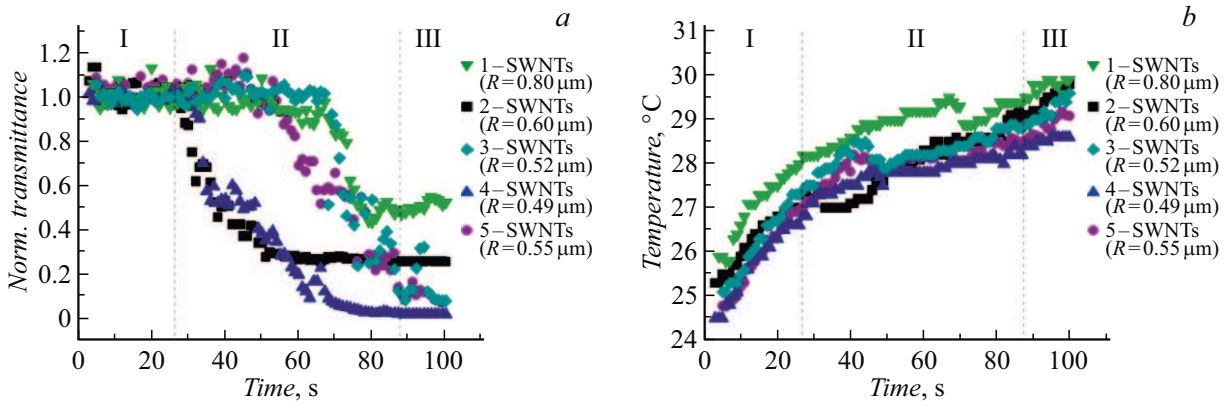

Figure 3. Two experimentally measured values versus time during laser photopolymerization of collagen/BSA/chitosan/eosin Y/SCNT/RGO dispersions: *a* — normalized optical transmittance; *b* — temperature.

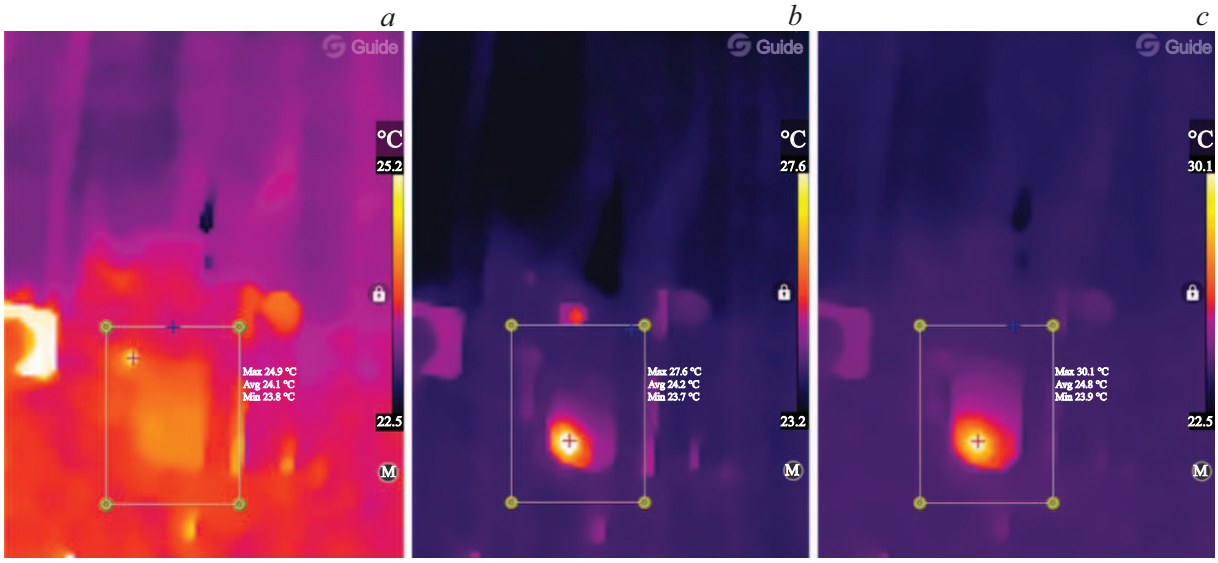

Figure 4. Images obtained by the thermal imager for all three areas during photopolymerization: *a* — initial moment of irradiation (zone I); *b* — photopolymerization occurs (zone II); *c* — heating of the photopolymerized area (zone III).

ization on the scanner system was subsequently performed at a higher radiation power, which made it possible to obtain such an effect in less time. In the first seconds, when radiation is applied to sample 1, the temperature rises to 28 °C without any structural changes in the sample (region I — Fig. 4, *a*), and then the temperature growth rate increased significantly and was less than 1 °C for 20 s, which was accompanied by a significant decrease in the normalized transmission down to 0.5 (region II — Fig. 4, *b*). After the hydrogel material had been formed, the temperature increase resumed at almost the same rate, but, after reaching a certain value, further growth stopped, and a stable equilibrium was established between the energy parameters of laserand temperature at exposure point (region III —Fig. 4, *c*). Similar pattern was observed for the other cases, too. Thus, hydrogel started to form at a temperature 27 °C and 27.5 °C in case of samples 2 and 3 accordingly. At the same time, there is a strong change in the normalized transmission to 0.1, which may indicate the formation of a dense structure. In case of sample 4 in region II the temperature varied at about 28 °C. At the same time, the lowest normalized transmission of 0.02 of all the studied samples is observed in the region III, which is evidence of the densest structure. In the case of sample 5, the obtained dependences of temperature and normalized transmission on time are close to sample 3. For samples 1, 3, and 5, photopolymerized sections were detached from the cuvette surface, which did not occur in the case of samples 2 and 4. For this reason, the change in normalized transmission occurred later and only some fluctuations in the values of normalized transmission were observed. This didn't influence determination of the optimal temperature, and later, a scanning system was used for photopolymerization in a vertical irradiation scheme, where the occurrence of such a phenomenon was excluded.

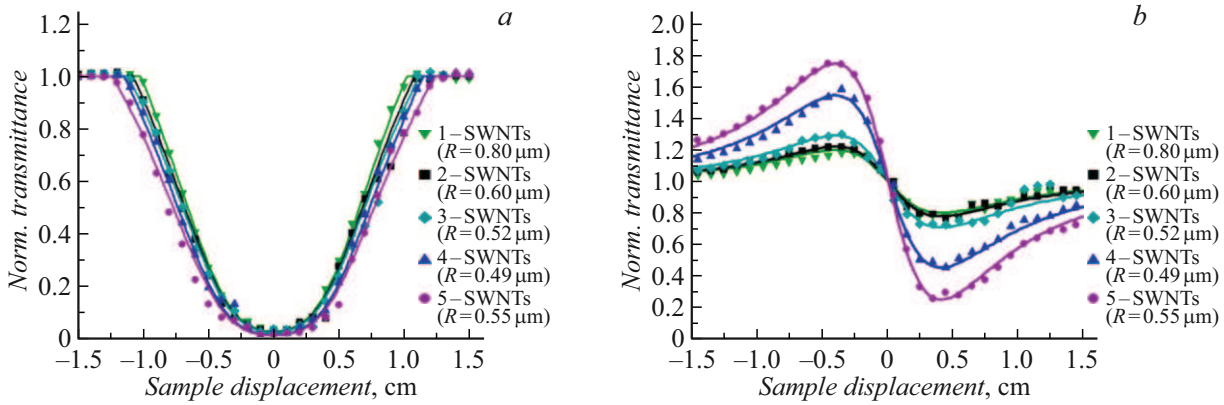

Figure 5. Results of Z-scanning with an open aperture of collagen/BSA/chitosan/eosin Y/SWCNT/RGO dispersions containing nanotubes with different hydrodynamic radius.

Table 2. Properties of dispersion (negative photoresist) collagen/BSA/chitosan/eosin Y/SWCNT/RGO

Variance (negative photoresist)	Hydrodynamic Radius SWCNT R, μm	Cross Section of a nonlinear absorption σ, GM	Threshold Exposure laser F_x, mJ/cm^2	Non-linear Index refraction n_n, cm^2/GW
1	0.80	750	90	0.25
2	0.60	770	80	0.25
3	0.52	760	80	0.40
4	0.49	850	70	0.80
5	0.55	830	60	1.00

The analyzed dependences of temperature and normalized optical transmission on the duration of laser photopolymerization, enabled to find the best possible temperature of the liquid biopolymer dispersion to ensure high reproducibility of the hydrogel characteristics obtained by photolithography. In case of sample 4, the laser radiation power is also used most effectively, as indicated by the value of the lowest normalized transmission after the formation of the composite hydrogel. Under the action of pulsed laser radiation with a sufficient pulse repetition period, a hydrogel is formed with an increase in volume due to the addition of other SWCNT and RGO forming a carcass, and the surface of carbon nanoparticles is modified as a result of interaction with albumin by analogy with the linear polymer [28].

2.3. Non-linear optical properties of dispersions for hydrogel fabrication

The cross section of the nonlinear absorption coefficient σ was obtained by Z-scanning [23,36] with an open aperture (Fig. 5, *a*) for five dispersions (negative photoresist). A decrease in the threshold exposure of laser radiation was found when nanotubes with a smaller hydrodynamic radius were used in the dispersion. The nonlinear refractive index was determined for all samples based on Z-scanning data with a closed aperture. Fig. 5, *b* shows the appropriate results.

The laser power during further photopolymerization was selected above the exposure threshold determined by Z-scanning (Table 2). At the same time, the power exceeded that used in determining the dependence of temperature on time. This is necessary to achieve photopolymerization at a movement rate of 240 mm/s at a single pulse energy of $\sim 100\,\mu$J. In accordance with the results of the studies of temperature dependence on irradiation time, the required temperature of the heating table was selected 28 °C.

The analysis of various factors impact on the further process of hydrogel photopolymerization was carried out according to optical parameters, the values of which are given in Table 2. During the use of nanotubes dispersion 1 with the largest characteristic hydrodynamic radius it exhibited a smaller cross-section of nonlinear absorption $\sigma = 750$ GM and the highest threshold exposure value $F_x = 90$ mJ/cm^2, while the refractive index was the lowest $n_n = 0.25$ cm^2/GW. In case of $2-4$ samples, there is a slight increase in the values of the nonlinear absorption cross section associated with an increase in the scattering capacity, which is confirmed by the calculated refractive index varying from 0.25 to 0.78 cm^2/GW. A tendency was also found to

decrease the laser threshold exposure from 1 to 5 samples, sufficient for the manifestation of nonlinear effects, which is explained by scattering, due to which the attenuation ability of the material increases faster. For a sample 5, which contains SWCNT with a characteristic hydrodynamic radius of 0.55 μm, this trend also persists, but the nonlinear absorption coefficient has, on the contrary, decreased, yet, within the calculation accuracy.

2.4. Resistivity and swelling of the hydrogel

Hydrogel samples were made in the form of squares 5×5 mm for measuring resistivity by a four-probe station using van der Pau method (Table 3). As a result, we managed to improve this characteristic by more than three times compared to the previously obtained value in our previous work (50 Ω·cm) [23]. The lowest resistivity was obtained in case of sample 4, in which SWCNT with a characteristic hydrodynamic radius of 0.49 μm were used. This results correlates well with the results of other studied optical characteristics. It is with this hydrogel composition-collagen/BSA/chitosan/eosin/SWCNT/RGO when the lowest normalized transmission was observed when exposed to laser pulses after 70 s irradiation, and the largest cross-section of nonlinear absorption was 850 GM (Table 2). This result shows the importance of controlling the ultrasonic processing, which allows to improve the characteristics to a certain value, while too long treatment can lead not only to beam splitting, but also to their shortening [40], which may result in deteriorated performance. For the nanotubes in hydrogel 4 the ultrasonic treatment was carried out for 80 min (Table 1).

Maintaining a temperature of about 28 °C allowed not only to carry out uniform polymerization, but also to create structures of complex shape (Fig. 6), which previously could not be created.

The fabricated hydrogel is capable of swelling to 200 %. At the same time, the obtained samples are poorly distinguishable from each other by this ability. The ability to retain moisture indicates the ability to maintain close contact with the nerve, while the material expands in volume.

Table 3. Resistivity of the formed hydrogel collagen/BSA/chitosan/eosin Y/SWCNT/RGO

Hydrogel	Hydrodynamic radius SWCNT R, μm	Specific resistivity, Ω·cm
1	0.80	36
2	0.60	56
3	0.52	32
4	0.49	14
5	0.55	38

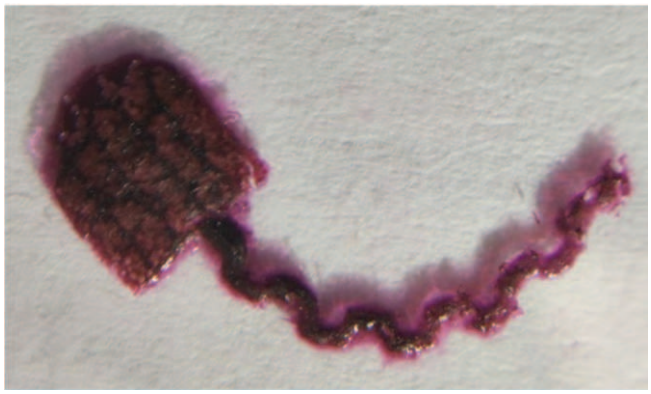

Figure 6. The structure of a complex shape made of hydrogel collagen/BSA/chitosan/eosin Y/SWCNT($R = 0.49\,\mu$m)/RGO (sample 4).

Conclusion

According to the study results, the possibility of forming a complex hydrogel at a temperature of 28 °C during photopolymerization of the hydrogel has been shown, which was previously not possible due to the presence of unpolymerized regions. The influence of two factors on the resistivity was found, namely, the characteristic hydrodynamic radius of the SWCNT, which can be used to assess the size of their beams, and the formation of their hybrid structures with RGO. The best values were obtained in case of sample 4 (collagen/BSA/chitosan/eosin Y/SWCNT/RGO) with SWCNT ($R = 0.49\,\mu$m). The resistivity here was 14 Ω·cm, which exceeded the earlier received value 50 Ω·cm.

The created conductive hydrogel material for use with electrodes is capable of increasing the efficiency of bionic devices, which are supposed to be used to replace or enhance the functions of sensory neurons by improving the operation stability while ensuring tight contact during swelling. Because of a hydrogel component and SWCNT the ions better penetrate inside and form a three-dimensional surface through which a charge is transmitted. The RGO plates in the material provide a larger contact area. As a result, the charge transfer area provided by a hydrogel with a structured system of RGO and SWCNT is significantly increased, thus allowing it to transfer a larger amount of charge at a lower voltage, and this will create necessary conditions for working with weak biosignals when stimulating the nerves.

Such hydrogels are being considered not only to increase the stability of platinum-iridium electrodes, but also to expand the possibilities for using materials such as titanium and medical steel alloys.

Funding

The work was performed under the state assignment of the Ministry of Education and Science of Russia (Project FSMR-2024-0003).

Acknowledgments

The work was performed using the equipment of the Center for Collective Use „Center for Laser Technologies in Medicine“ with the support of the Ministry of Science and Higher Education of Russian Federation (Agreement № 075-15-2025-669 of 05 August 2025)

Conflict of interest

The authors declare that they have no conflict of interest.

References

[1] T. Gordon. Int. J. Mol. Sci., **25** (1), 665 (2024). DOI: 10.3390/ijms25010665
[2] K. Kadan-Jamal, F. Wronowski, A. Jin, T.E. Naegele, V.R. Montes, X. Tao, A. Dominguez-Alfaro, C. Lee, G.G. Malliaras. Chem. Rev., **125** (15), 6874 (2025). DOI: 10.1021/acs.chemrev.4c00468
[3] E. Kim, S. Kim, Y.W. Kwon, H. Seo, M. Kim, W.G. Chung, W. Park, H. Song, D.H. Lee, J. Lee, S. Lee, I. Jeong, K. Lim, J. Park. Interdiscip. Med., **1** (2), e20230003 (2023). DOI: 10.1002/INMD.20230003
[4] L. Ni, Z. Yao, Y. Zhao, T. Zhang, J. Wang, S. Li, Z. Chen. Front. Neurol., **14**, 1081458 (2023). DOI: 10.3389/fneur.2023.1081458
[5] R. ElAbd, A. Alabdulkarim, S. AlSabah, J. Hazan, B. Alhalabi, S. Thibaudeau. Plast. Reconstr. Surg. – Glob. Open, **10** (3), e4115 (2022). DOI: 10.1097/GOX.0000000000004115
[6] S. Hasiba-Pappas, L.-P. Kamolz, H. Luze, S.P. Nischwitz, J.C.J. Holzer-Geissler, A.C. Tuca, T. Rienmüller, M. Polz, D. Ziesel, R. Winter. J. Pers. Med., **13** (3), 414 (2023). DOI: 10.3390/jpm13030414
[7] Q. Wang, Y. Zhang, H. Zhang, Z. Li. Neural Regen. Res., (2025). DOI: 10.4103/NRR.NRR-D-25-00553
[8] G.L. Schmidt. J. Am. Acad. Orthop. Surg., **27** (9), e401 (2019). DOI: 10.5435/JAAOS-D-17-00829
[9] T. Chu, Y. Xiao, H. Lai, L. Shi, Y. Cheng, J. Sun, Z. Pang, S. Cheng, K. Zhao, Z. Gao, R. Wang. ACS Nano, **19** (19), 18729 (2025). DOI: 10.1021/acsnano.5c03336
[10] W. Liu, Y. Luo, C. Ning, W. Zhang, Q. Zhang, H. Zou, C. Fu. J. Nanobiotechnol., **19**, 286 (2021). DOI: 10.1186/s12951-021-01031-y
[11] Y. Long, J. Li, F. Yang, J. Wang, X. Wang. Adv. Sci., **8** (8), 2004023 (2021). DOI: 10.1002/advs.202004023
[12] J. Ehlich, L. Migliaccio, I. Sahalianov, M. Nikic, J. Brodský, I. Gablech, X.T. Vu, S. Ingebrandt, E.D. Glowacki. J. Neural Eng., **19** (3), 036045 (2022). DOI: 10.1088/1741-2552/ac77c0
[13] A. Brown, N.J. Mandelberg, D. Munoz-Mendoza, V. Palys, P.C. Schalock, A. Mogilner, R. North, E.A. Petersen. Neural Interface, **24** (8), 1307 (2021). DOI: 10.1111/ner.13332
[14] A. Garcia-Sandoval, A. Pal, A.M. Mishra, S. Sherman, A.R. Parikh, A. Joshi-Imre, D. Arreaga-Salas, G. Gutierrez-Heredia, A.C. Duran-Martinez, J. Nathan, S.M. Hosseini, J.B. Carmel, W. Voit. J. Neural Eng., **15** (4), 045002 (2018). DOI: 10.1088/1741-2552/aab90d
[15] Y. Zhao, R. Sun, Z. Wang, S. Ma, R. Wang, F. Li, H. Geng. Engineer. Hydrogels as. ACS Appl. Bio Mater., **8** (9), 7587 (2025). DOI: 10.1021/acsabm.5c01269
[16] W.U. Khan, Z. Shen, S.M. Mugo, H. Wang, Q. Zhang. Chem. Soc. Rev., **54** (6), 2832 (2025). DOI: 10.1039/D4CS01074D
[17] L. Jiang, D. Gan, C. Xu, T. Zhang, M. Gao, C. Xie, D. Zhang, X. Lu. Small Sci., **5** (1), 2400362 (2025). DOI: 10.1002/smsc.202400362
[18] N.A. Staples, J.A. Goding, A.D. Gilmour, K.Y. Aristovich, P. Byrnes-Preston, D.S. Holder, J.W. Morley, N.H. Lovell, D.J. Chew, R.A. Green. Front. Neurosci., **11**, 748 (2018). DOI: 10.3389/fnins.2017.00748
[19] M. Wang, G. Mi, D. Shi, N. Bassous, D. Hickey, T.J. Webster. Adv. Funct. Mater., **28** (12), 1700905 (2018). DOI: 10.1002/adfm.201700905
[20] C.G.A. Lima, R.S. de Oliveira, S.D. Figueiro, C.F. Wehmann, J.C. Goes, A.S.B. Mater. Chem. Phys., **99** (2−3), 284 (2006). DOI: 10.1016/j.matchemphys.2005.10.027
[21] A.Y. Gerasimenko, U.E. Kurilova, M.S. Savelyev, D.T. Murashko, O.E. Glukhova. Compos. Struct., **260**, 113517 (2021). DOI: 10.1016/j.compstruct.2020.113517
[22] X. Wei, S. Li, W. Wang, X. Zhang, W. Zhou, S. Xie, H. Liu. Adv. Sci., **9** (14), 2200054 (2022). DOI: 10.1002/advs.202200054
[23] M.S. Savelyev, A.V. Kuksin, D.T. Murashko, E.P. Otsupko, V.V. Suchkova, K.D. Popovich, P.N. Vasilevsky, Y.O. Vasilevskaya, U.E. Kurilova, E.M. Eganova, P.A. Edelbekova, S.V. Selishchev, A.A. Pavlov, A.Y. Gerasimenko. Polymers (Basel), **17** (10), 1300 (2025). DOI: 10.3390/polym17101300
[24] S.K. Debnath, R. Srivastava. Front. Nanotechnol., **3**, 644564 (2021). DOI: 10.3389/fnano.2021.644564
[25] K. Pieklarz, M. Tylman, Z. Modrzejewska. Mini-Reviews Med. Chem., **20** (16), 1619 (2020). DOI: 10.2174/1389557520666200513120407
[26] F. Valentini, E. Mari, A. Zicari, A. Calcaterra, M. Talamo, M.G. Scioli, A. Orlandi, S. Mardente. Int. J. Mol. Sci., **19** (5), 1316 (2018). DOI: 10.3390/ijms19051316
[27] A.Y. Gerasimenko, A.V. Kuksin, Y.P. Shaman, E.P. Kitsyuk, Y.O. Fedorova, D.T. Murashko, A.A. Shamanaev, E.M. Eganova, A.V. Sysa, M.S. Savelyev, D.V. Telyshev, A.A. Pavlov, O.E. Glukhova. Nanomaterials, **12** (16), 2812 (2022). DOI: 10.3390/nano12162812
[28] M.S. Savelyev, N.O. Agafonova, P.N. Vasilevsky, D.I. Ryabkin, D.V. Telyshev, P.S. Timashev, A.Y. Gerasimenko. Opt. Eng., **59** (6), 1 (2020). DOI: 10.1117/1.OE.59.6.061623
[29] E.I. Nagaev, I.V. Baimler, A.S. Baryshev, M.E. Astashev, S.V. Gudkov. Molecules, **27** (19), 6752 (2022). DOI: 10.3390/molecules27196752
[30] H. Choi, J. Seok Woo, J. Tark Han, S.-Y. Park. Nanotechnology, **28** (46), 465706 (2017). DOI: 10.1088/1361-6528/aa8c24
[31] G.F. Gabidinova, G.A. Timerbulatova, A.G. Daminova, S.F. Galyaltdinov, A.M. Dimiev, M.A. Kryuchkova, R.F. Fakhrullin, L.M. Fatkhutdinova. Hyg. Sanit., **101** (12), 1509 (2023). DOI: 10.47470/0016-9900-2022-101-12-1509-1520
[32] A.V. Korchun, E.Y. Evshchik, S.A. Baskakov, O.V. Bushkova, Y.A. Dobrovolsky. Chim. Techno Acta, **7** (4), 259 (2020). DOI: 10.15826/chimtech.2020.7.4.21

[33] A.Y. Kurmysheva, O. Yanushevich, N. Krikheli, O. Kramar, M.D. Vedenyapina, P. Podrabinnik, N.W. Solís Pinargote, A. Smirnov, E. Kuznetsova, V.V. Malyavin, P. Peretyagin, S.N. Grigoriev. Gels, **9** (9), 680 (2023). DOI: 10.3390/gels9090680
[34] E.G. Pogorelov, A.I. Zhbanov, Y.-C. Chang, S. Yang. Langmuir, **28** (2), 1276 (2012). DOI: 10.1021/la203776x
[35] S. Hwang, D. Lee, S.-Y. Ju. J. Mol. Liq., **435**, 128144 (2025). DOI: 10.1016/j.molliq.2025.128144
[36] A. Ajami, W. Husinsky, R. Liska, N. Pucher. J. Opt. Soc. Am. B., **27** (11), 2290 (2010). DOI: 10.1364/JOSAB.27.002290
[37] A.Y. Tolbin, M.S. Savelyev, P.N. Vasilevsky, A.Y. Gerasimenko. Phys. Chem. Chem. Phys., **26** (11), 8965 (2024). DOI: 10.1039/D4CP00055B
[38] M. Sheik-Bahae, A.A. Said, T.-H. Wei, D.J. Hagan, E.W. Van Stryland. IEEE J. Quant. Electron., **26** (4), 760 (1990). DOI: 10.1109/3.53394
[39] M. Yang, L. Wang, W. Liu, W. Li, Y. Huang, Q. Jin, L. Zhang, Y. Jiang, Z. Luo. Nat. Commun., **15** (1), 7993 (2024). DOI: 10.1038/s41467-024-52418-y
[40] H. Rennhofer, B. Zanghellini. Nanomaterials, **11** (6), 1469 (2021). DOI: 10.3390/nano11061469
[41] K. Matsumoto, T. Takahashi, Y. Jinguji, M. Jikei. Int. J. Soc. Mater. Eng. Resour., **22** (1−2), 20 (2017). DOI: 10.5188/ijsmer.22.20

Translated by T.Zorina